Partial Discharge Evolution Mechanism in DBC of High-Voltage Power Electronics Modules Under Rectangular-Wave Voltage in Transitional Time Scale

Zhaocheng Liu, Xiang Cui, *Senior Member, IEEE*, Xuebao Li, Weitong Xu, Zhibin Zhao, and Lei Qi

***Abstract*—Insulation of high-voltage wide-bandgap module faces significant challenges in applications. However, there is little research on evolution characteristics of partial discharge (PD) during the transitional time scale—when PD behavior evolves from initial transient phenomena toward long-term steady-state conditions. This research is meaningful for insulation reliability of high-voltage module. To this end, PD evolution characteristics and mechanism of typical structure [direct bonded copper, (DBC)] in high-voltage module during the transitional time scale are analyzed in this article. First, by shunt-resistor-based current measurement, evolution process of detailed PD characteristics is collected. Furthermore, the transient electric field considering relaxation effect during the transitional period is simulated for analysis. Moreover, an analytical formula of the PD pulse current under the rectangle-wave voltage is proposed for the first time, which establishes a bridge between PD detailed characteristics and electric field. Finally, combining electric field simulation results and the proposed analytical formula, the mechanism explanation of PD evolution characteristics under rectangular-wave voltage is proposed, which corresponds well with experimental results. More importantly, the explanation points out that the change of electric field caused by relaxation effect is main reason for the evolution of PD characteristics.**

***Index Terms*—DBC structure, partial discharge (PD), rectangle-wave voltage, relaxation effect.**

I. Introduction

HIGH-VOLTAGE wide-bandgap devices are widely regarded as the next generation of high-voltage power electronic devices, due to their high breakdown strength, high thermal conductivity, and high switching speed, which has broad application prospect [1], [2], [3].

However, the high-voltage module insulation faces significant challenges in realistic application [3], [4]. As shown in Fig. 1, it is a typical structure of high-voltage module.

Received 19 June 2025; revised 18 September 2025; accepted 31 October 2025. Date of publication 7 November 2025; date of current version 19 January 2026. This work was supported by the National Outstanding Youth Science Fund Project of National Natural Science Foundation of China under Grant 52225701. Recommended for publication by Associate Editor C. Zhan. *(Corresponding author: Xuebao Li.)*

The authors are with the State Key Laboratory of Alternate Electrical Power System with Renewable Energy Sources, Beijing 102206, China (e-mail: lxb08357x@ncepu.edu.cn).

Color versions of one or more figures in this article are available at https://doi.org/10.1109/TPEL.2025.3630160.

Digital Object Identifier 10.1109/TPEL.2025.3630160

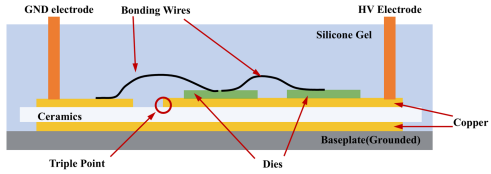

Fig. 1. Typical structure of high-voltage module [13].

Numerous studies and experimental results have confirmed that the direct bonded copper (DBC) structure—typically composed of a ceramic substrate such as Al_2O_3, sandwiched between bonded copper layers—is one of the primary insulation weak points [4], [5], [6], [7]. The frequent occurrence of PDs at the interface between DBC structure and silicone gel limits the enhancement of insulation capacity in high-voltage module and poses a serious threat to their reliability [6], [7], [8].

Moreover, high-voltage module operates under positive polarity rectangle-wave voltage. Under this electrical stress, its partial discharge (PD) characteristics have been shown to differ significantly from those observed under conventional ac or dc conditions [8], [9], [10], [11]. As a result, to better understand the insulation characteristics of DBC in high-voltage module under actual operating conditions, it is essential to investigate the discharge behavior of the DBC structure under such electrical stress.

In recent years, many scholars have researched the discharge phenomenon of DBC structure under positive polarity rectangle-wave voltage. Zeng et al. [12] pointed out the triple point (intersection of three materials) is the maximum electric position. Liu et al. [13] explained the PD mechanism and discharge pattern under the short-term positive polarity rectangle-wave voltage. Furthermore, Li et al. [14], You et al. [15], and You et al [11] revealed the influence of voltage amplitude, *dV/dt*, rise time, frequency, and duty of positive polarity rectangle-wave voltages on the short-term PD characteristics of DBC structure, respectively. Besides, in 2025, Ding et al. [16] reported the insulation aging characteristics of DBC by using UHF antenna method under long-term positive repetitive rectangle-wave voltage.

In the existing studies, most of the research focuses either on the initial inception stage under short-term stress [17], or on steady-state behavior under long-term stress, such as electrical

treeing, which has been identified as a critical contributor to insulation aging [7]. More recently, researchers have gradually recognized the importance of insulation research of DBC structures under the transitional time scale—when the electric field or other insulation characteristics evolve from initial transient phenomena toward long-term steady-state conditions [18], [19]. During this transitional period, studies have shown that dielectric relaxation can gradually distort the local electric field, thereby accelerate space-charge accumulation and promote insulation degradation [18]. However, there is little experimental research about insulation characteristics (for example, PD evolution characteristics) of DBC structures during the transitional time scale. Moreover, the regularities of detailed parameters of PD waveform and the corresponding PD mechanism are still unknown during this transitional period under positive polarity rectangle-wave voltage. Yet, it is precisely during this transitional period that critical changes in discharge behavior can be significantly related to the insulation reliability and lifetime of the high-voltage module [20], [21]. Therefore, revealing the PD evolution characteristics during this time scale is of great significance for accurately evaluating the insulation reliability of high-voltage modules.

In order to address above gaps, this article investigates the detailed PD evolution characteristics and underlying discharge mechanisms during the transitional period. A shunt-resistor-based current measurement system is employed to capture and record PD detailed waveform and evolution characteristics. The PD pulse characteristics, including waveform parameters and discharge patterns during the transitional period, are systematically analyzed first. Then, transient electric field distribution within the DBC structure during the transitional period is simulated. Moreover, based on charge transport dynamics, the effects of electric field distribution and material parameters on PD waveform characteristics are explored through a proposed one-dimensional analytical model. Furthermore, combining electric field simulation results and the analytical formula, the PD evolution mechanism during the transitional period is proposed, which corresponds well with experimental observations. Moreover, the key point leading to the evolution process is also analyzed. This article provides valuable insights and references for insulation analysis of DBC structures in high-voltage modules.

II. Experimental Setup

A. Preparation of Samples

The samples used in the experiment are consistence with the actual structure. As shown in Fig. 2, the DBC structure is composed of Al_2O_3 ceramic plate (1 mm thickness) and Cu/Ni/Au metal layers. The thickness of Cu, Ni and Au are 0.25 mm, 1 μm and 0.1 μm, respectively. Before being sealed by the silicone gel, the DBC structure is put into the transparent acrylic container. The HV electrode is connected to the front side middle metal layer of DBC and the GND electrode is connected to the front side bottom metal layer of DBC. Moreover, the metal layer of rear side of DBC is also connected to the GND electrode by Cu foil. In this case, the voltage is mainly applied between the middle metal layer and bottom metal layer of front side of

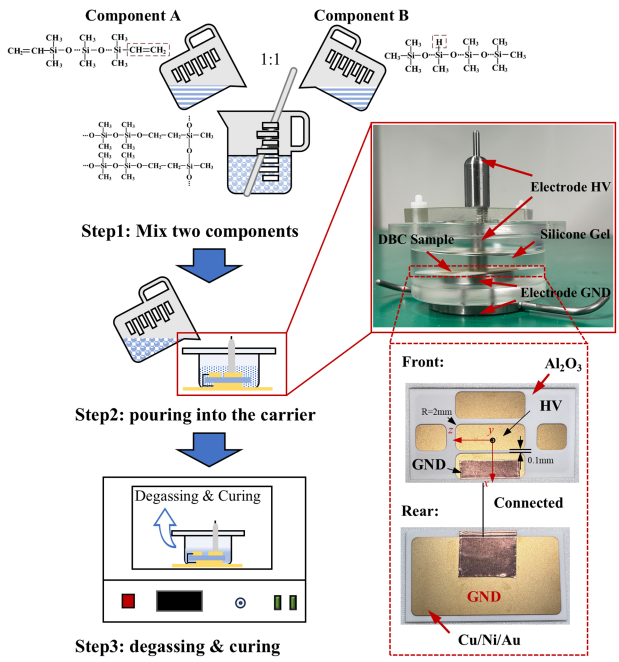

Fig. 2. Sample structure and its preparation process.

TABLE I
Model Parameters of Dielectric Materials [23]

Material	Permittivity(F/m)	Conductivity(S/m)
Al_2O_3	$9 \times 8.854 \times 10^{-12}$	10^{-12}
Silicone gel	$2.7 \times 8.854 \times 10^{-12}$	10^{-13}

DBC structure. The length between these two electrodes is 0.1 mm.

After connecting the metal layers to the electrodes, the silicone gel is prepared in a beaker by stirring component A and component B of silicone gel with mass ratio of 1:1. During this process, under the action of the platinum catalyst, hydrogen is added to vinyl, and the Si-H bond is converted into the Si-C bond so that the linear siloxane is crosslinked to form a polymer network [22]. Moreover, there are a large number of bubbles generated in this process because of stirring. Then, the silicone gel is poured into the transparency acrylic container. After that, in order to eliminate the bubbles, the transparency acrylic container is put in the vacuum chamber and degassed according to the degassing curve under room temperature. Finally, the transparency acrylic container is placed into the incubator and kept at 80 °C for 4 h [22]. Corresponding parameters of silicone gel and Al_2O_3 ceramic plate are given in Table I. The silicone gel parameters were obtained dielectric spectroscopy measurements using a Novocontrol broadband dielectric spectrometer with interdigitated electrodes, while the Al_2O_3 ceramic parameters were taken from the manufacturer's datasheet.

B. Experiment Platform

The experimental platform for PD detection based on the shunt-resistor-based current measurement method is illustrated in Fig. 3. The platform is placed in an electromagnetic shielded

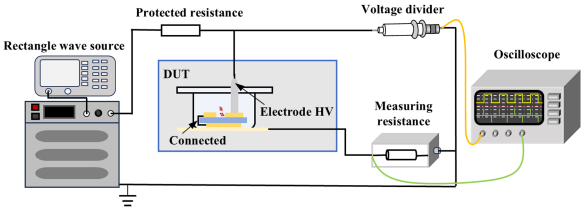

Fig. 3. Experiment platform of detection of PD under rectangle-wave voltage.

room, the power supply and ground in this room are specially design and hence external electromagnetic interference is negligible. The rectangle-wave voltage power supply consists of a signal generator (Tektronix AFG3200C, output range −10 V to +10 V with a nanosecond-scale rise time) and a high-voltage amplifier (Matsusada AMP-40B20, amplification factor of 4000, maximum output ±40 kV, maximum current 20 mA, frequency bandwidth dc–5 kHz). The signal generator produces a rectangle-wave voltage, which is then amplified by the high-voltage amplifier, resulting in a high-voltage rectangle-wave output. The output of the amplifier is connected to the protective resistor through a specially designed 2 m high-voltage cable, whose parasitic capacitance is minimal and can be regarded as negligible. Moreover, the protective resistor is a non-PD resistor with a value of 10 kΩ. Additionally, the experimental sample is grounded through the non-inductive sampling resistor with a value of 500 Ω which is enclosed in a custom metal shielding box to suppress electromagnetic coupling Overall, the platform has been verified to remain PD-free under an applied voltage of at least 30 kV.

As for the measurement system, the voltage applied to the DUT is measured using a high-voltage divider, which features a measurement range of −40 kV to +40 kV with an attenuation ratio of 1000:1, a measurement accuracy below 1.5%, and a frequency bandwidth ranging from dc to 140 MHz. The PD pulse is measured through the sampling resistor by a broadband voltage probe identified as Teledyne LeCroy PP-022 with bandwidth ranging from dc to 500 MHz. In this experimental setup, the positive direction of positive polarity of PD pulse current is from HV electrode to GND electrode. In addition, in the experiments, rectangle-wave voltage and the current pulse signals can be collected by the oscilloscope whose maximum sampling rate can reach 10 GS/s.

C. Experiment Procedure

In this experiment, the frequency and duty of rectangle-wave are set 50 Hz and 50%, respectively. As for the overshooting of rectangle-wave voltage, the variation time is 0.05 ms for each rise and fall edge and then 9.95 ms for steady time. Because the size and materials of sample are fixed, the partial discharge inception voltage (PDIV) of this sample under corresponding repetitive rectangle-wave voltage is measured according to the standard [24]. More details about PDIV tests can be found in [13]. The experiment results are given in Table II. After multiple measurements of multiple samples and fitting to a Weibull

TABLE II
PD INCEPTION VOLTAGE RESULTS

Times	1	2	3	4	5	6	7
PDIV(kV)	9.02	9.02	9.38	10.8	11.23	11.19	11.53
$PDIV_{63\%}$(kV)				10.51			

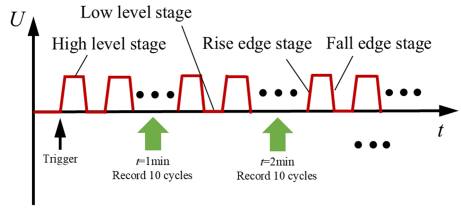

Fig. 4. Applied positive polarity repetitive rectangle-wave voltage and collect method.

distribution, the PDIV of this structure with a probability of occurrence of 63% is 10.51 kV.

As for the measurement of PD evolution characteristics during the transitional period under the room temperature (25°C), the waveform of applied positive polarity rectangle-wave voltage is shown in Fig. 4. Before triggering, there is no voltage. After triggering, PD pulse current signals are recorded once every minute, with each recording capturing a 0.2-s waveform segment to measure the PD evolution characteristics. Moreover, the four typical stages of rectangle-wave are also defined in Fig. 4.

Furthermore, the amplitude of the rectangle-wave is set to 10 kV, which is slightly below the PDIV threshold to avoid the breakdown and other defects. Besides, the sample used for evolution measurement that have not been subjected to any prior PD tests to prevent damage to the sample by the prior PD tests. Other parameters of applied positive polarity rectangle-wave voltage are same as above measurement of PDIV.

III. Experiment Results of PD of DBC Over Time Under Positive Polarity Rectangle-Wave Voltage

A. Extraction Method of PD Pulse

Because the capacitor effect of the sample cannot be ignored under the rectangle-wave voltage, there is large amplitude displacement current at rise and fall edge stages. Though the current pulse signal is acquired, the presence of displacement current hinders the extraction of PD pulse current. At present, there are extraction methods assisted by optical signals and electromagnetic wave [17]. These methods will increase the additional storage amount and time cost, which is not cost-effective.

Our group proposed an automatic extraction method from the current pulse signal without other assisted signals in 2023 [25]. The automatic extraction method serves as a post-processing procedure to remove the influence of displacement current from the raw signal. The detailed process is as follows.

1) According to the sampling rate, an appropriate time window is selected to perform Gaussian filtering on the original current waveform i_0, resulting in a smoothed waveform i_1. The Gaussian filter effectively suppresses

TABLE III
STATISTIC OF NUMBER OF PD PULSES OVER TIME

No. of per 10 cycles	1	2	3	4	5	6	7	8	9	10	11	12	13	14	15	16	17	18
Total Pulse Number	105	79	102	112	102	108	110	115	113	109	110	102	103	107	111	112	106	103
Positive Pulse Number	52	39	49	57	50	50	52	53	55	51	54	52	49	51	51	52	50	51
Negative Pulse Number	53	40	53	55	52	58	58	62	58	58	56	50	54	56	60	60	56	52

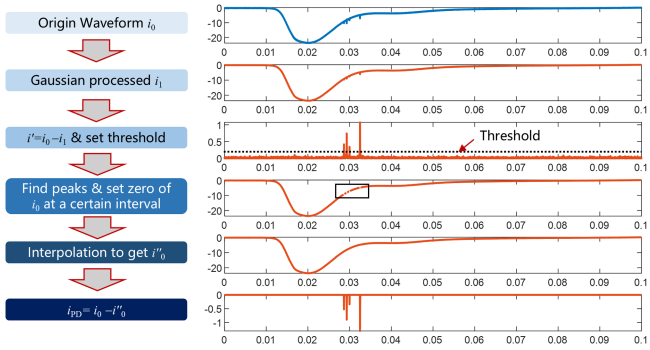

Fig. 5. Process of extraction method of PD.

high-frequency noise and local PD pulses while preserving the low-frequency displacement current component.

2) The difference between the original signal and the smoothed waveform is calculated as $i' = i_0 - i_1$. The waveform i' mainly contains distorted PD pulses and residual high-frequency noise.
3) A threshold is then set to detect the local extrema in i' whose amplitudes exceed the noise level, and their time positions are recorded as $t_{p,m}$ ($m = 1, 2, \ldots, M$, where M is the number of PD pulses).
4) For each detected pulse position $t_{p,m}$, the corresponding segments of i_0 within ± 0.15 μs are set to zero, producing a component i'_0. The window width (± 0.15 μs) is an engineering parameter that only needs to be larger than twice the typical pulse width of the PD signal to ensure complete removal of the PD components.
5) The zeroed segments in i'_0 are then reconstructed by shape-preserving piecewise cubic spline interpolation using the adjacent nonzero data, yielding a continuous low-frequency waveform i''_0.
6) Finally, the displacement-current-free PD waveform is obtained as $i_{PD} = i_0 - i''_0$.

The overall workflow is illustrated in Fig. 5, and the effectiveness of this method in separating the four stages of the rectangle wave excitation is shown in Fig. 6.

B. Basic Characteristics of PD Pulse Over Time

By using the extraction method, the PD pulse waveform can be extracted. In this case, 10 cycles of PD pulse waveform (0.2 s) can be acquired for each minute. Compared with minute scale, the parameters of PDs in these 10 cycles (0.2s) can be seen basically unchanged.

For sake of analysis, PD signals over ten cycles are mapped onto single voltage cycle based on their amplitude and phase, which can be seen as phase resolved partial discharge (PRPD) diagram, as illustrated in Fig. 7(a). Moreover, the statistic of number of PD pulses for each minute is given in Table III.

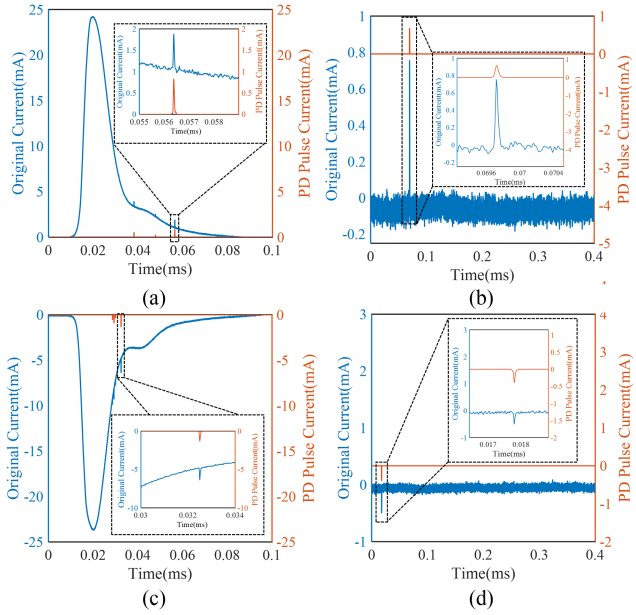

Fig. 6. Effectiveness of extraction method. (a) Rise edge stage. (b) High-level stage. (c) Fall edge state. (d) Low-level stage.

It can be found that most of PD pulses accumulate at rise and fall edges stages of voltage waveform and hence these PD pulses can be used for the statistical analysis. Moreover, the polarity of PD at rise edge stage is positive and at fall edge stage is negative. It can be found that the amplitude of PD increases for both positive and negative PDs during transitional period. Besides, the number of PD pulses is basically unchanged and hence the influence of number of PD is ignored in the following analysis.

In order to show discharge characteristics clearly, enlarge figures at rise and fall edges of Fig. 7(a) are given in Fig. 7(b) and (c), respectively. The black and blue dots indicate the centroid (mean values) of the points formed by the discharge amplitude-phase coordinates for Fig. 7(b) and (c), respectively. For PDs at rise edge stage (positive PDs) as shown in Fig. 7(b), the amplitude of PDs over time increases gradually at first and then reaches a stable state. At the same time, the discharge amplitude-phase coordinates of the PDs are initially relatively concentrated but gradually become more dispersed. Besides, the mean value of phase of PDs gradually shifts to the right and then fixes. As for PDs at fall edge (negative PDs) shown in Fig. 7(c), as time progresses, the discharge phases remain relatively concentrated, while only the amplitude increases, resulting in a pattern resembling the digit "1." Moreover,

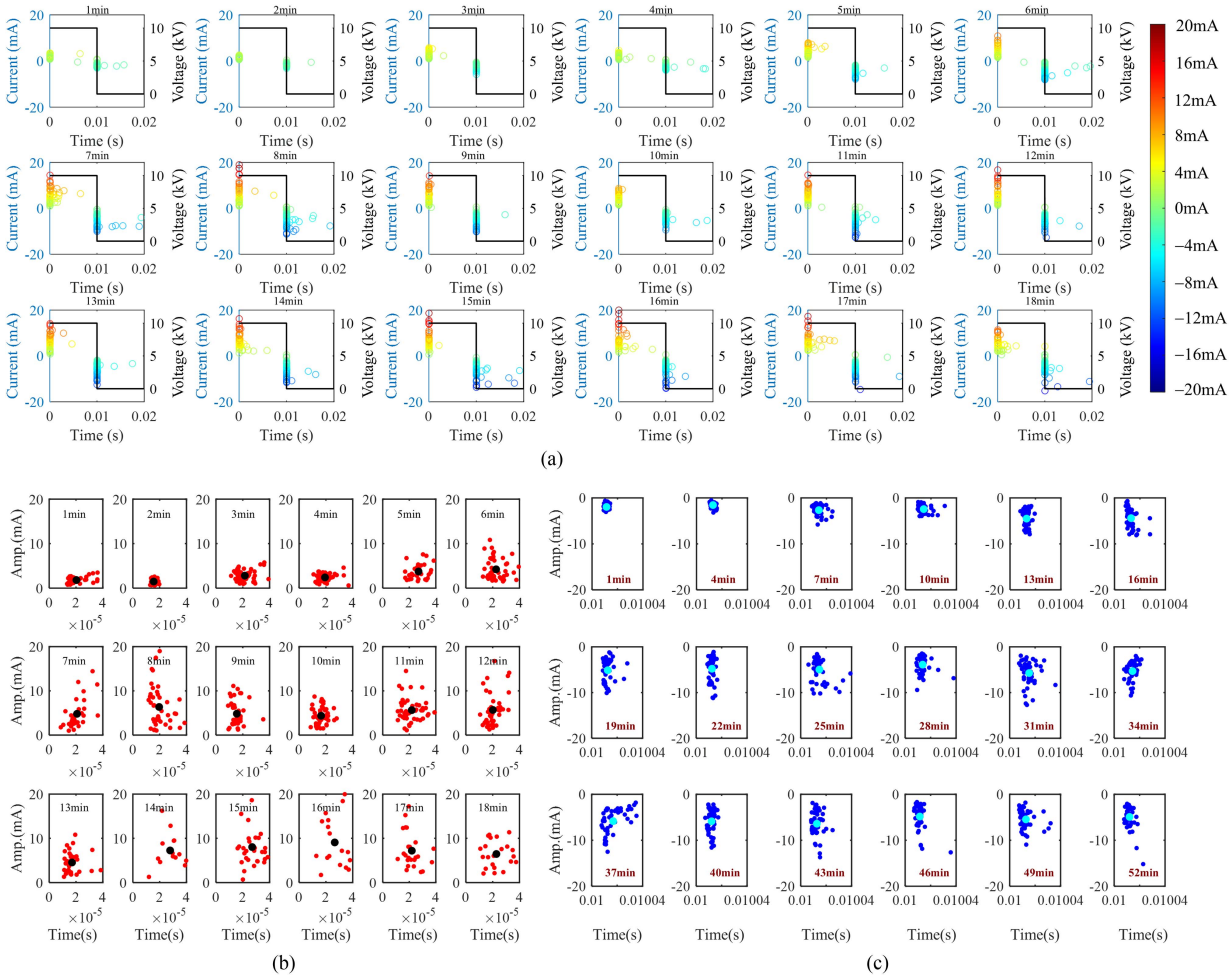

Fig. 7. PRPD diagram of PDs of DBC over time. (a) PRPD diagram over time. (b) Enlarge figure of rise edge stage (c) Enlarge figure of fall edge stage.

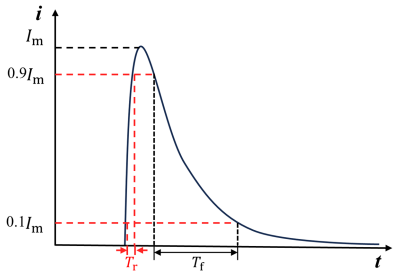

Fig. 8. Parameters of PD waveform.

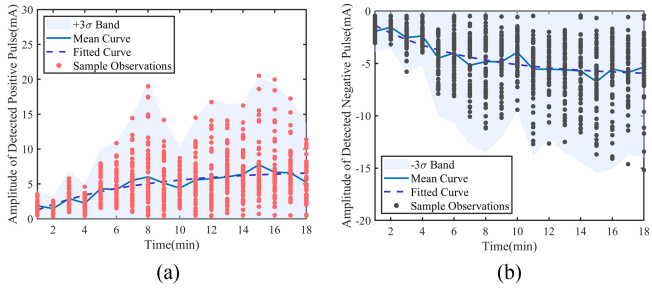

Fig. 9. Characteristic of amplitude of discharge pulse over time. (a) Positive polarity. (b) Negative polarity.

the mean value of phase of PDs is basically unchanged over time.

C. Detailed Characteristics of PD Pulse Over Time

Furthermore, the detailed characteristics of PD pulses are quantitatively analyzed in this subsection. The typical PD pulse current is given in Fig. 8. Moreover, the typical waveform parameters of PD pulse current, such as amplitude I_m, rise time T_r and fall time T_f are defined in Fig. 8.

The average amplitudes of positive and negative PD pulse at each 10 cycles over time are given in Fig. 9(a) and (b), respectively. Besides, the 3σ or -3σ confidence interval is also provided, where σ is the standard deviation for statistic variable. It can be found that amplitudes of positive and negative PD pulses both increase over time initially. After about 9 min, the amplitudes of positive and negative PD pulse gradually become unchanged.

Besides, the average values of rise time, and fall time for every ten cycles over time are given as red and black lines in Fig. 10.

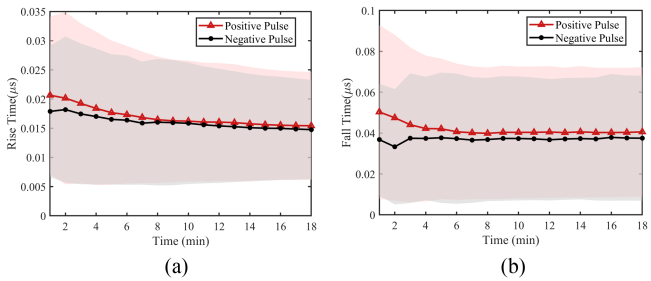

Fig. 10. Characteristic of rise and fall time of discharge pulse over time. (a) Rise time. (b) Fall time.

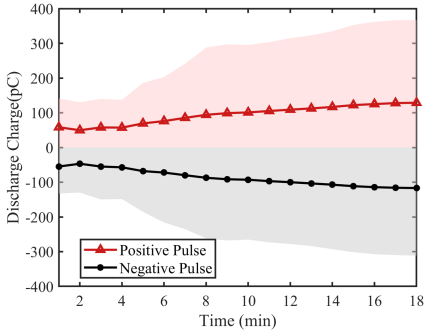

Fig. 11. Characteristic of apparent charge over time.

Moreover, the $\pm\sigma$ confidence intervals are also given with the same color shades.

As shown in Fig. 10(a), the rise times for both positive and negative PD pulses exhibit exponential decay over time and the change gradually levels off after 9 min. As for the fall time shown in Fig. 10(b), the fall time of positive pulses exhibits exponential decay over time and the change gradually levels off after 9 min, but the fall time for negative pulse is basically unchanged over time.

Furthermore, by the extraction method shown in Fig. 5, the extracted PD current signals within each 0.2 s segment recorded every minute can be acquired. Then, by integrating the positive and negative PD pulse over time separately, the apparent charge can be acquired. The average values of apparent charge for ten cycles over time is given in Fig. 11. Similarly, the same color $+\sigma$ or $-\sigma$ confidence intervals are also given. It can be found that the positive and negative discharge charge increases quickly before 9 min and then increases slowly. Moreover, the charge quantity for negative and positive pulses are basically the same.

IV. Evolution Mechanism of PD Over Time

In the previous section, the evolution of detailed PD parameters during the transitional period was observed, despite the externally applied voltage waveform and other experimental conditions remaining unchanged. This suggests that certain variables associated with PD behavior change over time. Because PD is strongly correlated with the electric field strength, the electric field relaxation process—an intrinsic property of insulating materials—is introduced in an attempt to analyze these evolution characteristics.

Section IV-A focuses on numerical simulation of the transient electric field, explicitly considering dielectric relaxation effects. Section IV-B establishes the quantitative relationship between local PD waveform characteristics and the electric field. After that, Section IV-C applies this framework (see Section IV-A and Section IV-B) to analyze the evolution behavior of PD pulses parameters.

A. Simulation of Transient Electric Field of DBC

In the existing simulation about PD mechanism under short-term or long-term positive polarity rectangle wave voltage, only the electrostatic field or steady electric current field is simulated. However, in practice, during the transitional period, there is electric field relaxation process (Maxwell–Wagner effect), which is also an evolution process related to the materials parameters and structure.

According to Table I, there are both leakage current property and dielectric property of ceramic and silicone gel of sample shown in Fig. 2. From the perspective of circuit, the structure of sample can be regarded as a complex *RC* network. Moreover, the electric field can be regarded as the result of a complex *RC* network response under the voltage waveform shown in Fig. 4. Under the stress shown in Fig. 4, there will be a transient process of complex *RC* network response after triggering and then response gradually transforms to steady state under the periodic rectangle-wave. It means that the electric field of initial several cycles is significantly different from the electric field after long-term work despite the unchanged voltage waveform. This transition is referred to as the electric field relaxation process, also known as the Maxwell–Wagner relaxation effect [21].

Therefore, it can be found that the transient electric field is controlled not only by the externally applied voltage, but also by the relaxation process induced by the material properties and structure. In this section, an evolution of the electric field considering the Maxwell–Wagner effect under the positive polarity rectangle-wave voltage is simulated.

According to Fig. 2, the structure extends much longer along the *z*-dimension compared to the *x*–*y* cross section. Owing to this large aspect ratio, the electric field along the *z*-direction is very small and can be considered negligible, allowing the overall field distribution to be regarded as two-dimensional. So, in the simulation, the geometry of DBC structure is established in Fig. 12. Moreover, there is the 0.03 mm fillet at triple points A and B.

In order to consider the leakage and dielectric properties, the equation calculated in dielectric materials such as, silicone gel and Al_2O_3 is

$$\nabla \cdot \left(\gamma \nabla \varphi + \varepsilon \frac{\partial \nabla \varphi}{\partial t}\right) = 0 \tag{1}$$

where, γ and ε are the conductivity and permittivity of materials, φ is potential and t is time. The parameters of materials are given in Table I. It can be estimated the relaxation time is about minute-scale.

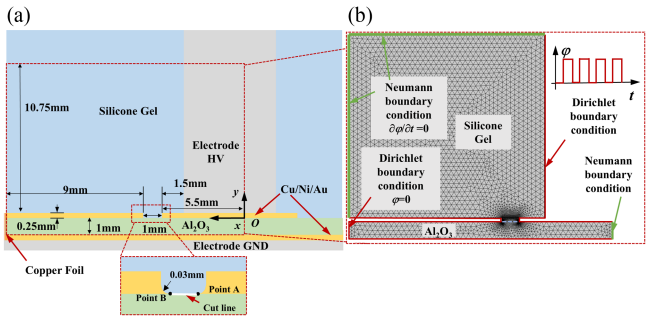

Fig. 12. The simulation model. (a) Geometry of simulation structure. (b) Mesh and boundary conditions of simulation.

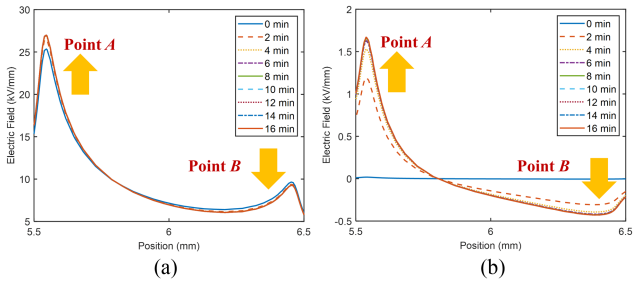

Fig. 13. Transient electric field E_x distribution of DBC. (a) End moment of rise edge stage. (b) End moment of fall edge stage.

As for the interfaces between metal electrode and dielectric materials, they are treated as Dirichlet boundary condition while other boundaries are set homogeneous Neumann boundary condition. For the GND electrode, the potential is set 0. While for HV electrode, the rectangle-wave voltage is set as shown in Fig. 4 and the duration time of simulation is 1000 s.

As mentioned in the introduction, the triple points are usually maximum electric field positions. In this structure, because external voltage is applied along the x-direction, the electric field is dominated by its tangential component, which is lies along the x-direction. In this case, the tangential component of electric field E_x at the silicone gel side is mainly analyzed, whose positive direction is along the x-axis. The electric field E_x at the interface (silicone gel side) of the triple points along cut line indicated in Fig. 12 is extracted and presented in Fig. 13. Fig. 13(a) shows the transient electric field distribution at the end moment of rise edge stage while Fig. 13(b) corresponds to the end moment of fall edge stage. Furthermore, the temporal evolution of the electric field strength at points A and B in Fig. 12 is illustrated in Fig. 14.

As for the evolution of electric field at the end moment of rise edge stage of each cycle, as shown in Fig. 14(a) and (c) the directions of electric field E_x at point A and B are the same. Moreover, the electric field amplitude at point A is much larger than that of point B. As time progresses, the electric field amplitude at point A increases while at point B decreases over time initially and then they are both basically unchanged after 450 s.

As for the evolution of electric field at the end moment of fall edge stage of each cycle, as shown in Fig. 14(b) and (d), the directions of electric field E_x at points A and B are opposite.

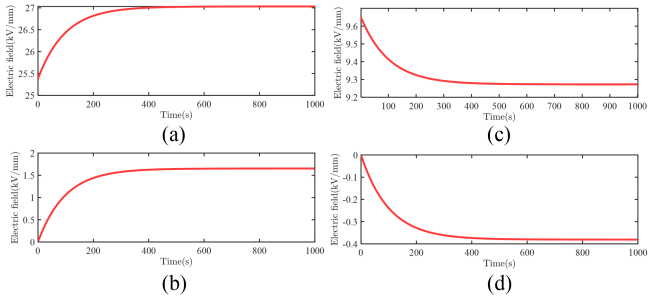

Fig. 14. Transient electric field E_x over time. (a) At each end moments of rise edge stages at point A. (b) At each end moments of fall edge stages at point A. (c) At each end moments of rise edge stages at point B. (d) At each end moments of fall edge stages at point B.

Moreover, the electric field amplitude at point A is still larger than that of point B, but the electric field amplitude at point A and B are both much lower than that at end moment of rise edge stage. Besides, the electric field amplitude at points A and B both increase over time and then are basically unchanged after 450 s.

From these results, it can be found that there is the evolution of electric field over time caused by the Maxwell–Wagner effect. Besides, the relaxation time of electric field strength at points A and B are both basically unchanged after 450 s which is similar to transitional time scale in experimental results. This indicates that the relaxation behavior of the electric field may serve as a possible explanation for the observed PD characteristics during the transitional period.

B. Analytical Equations of Charge Transport Mechanism

In this section, the relationship between electric field and PD waveform characteristics is explored under charge transport dynamics. In this case, the transient electric field $E(t)$ is considered in the derivation. Moreover, Besides, the spatial scale of PD transport process is only nanometer to micrometer, and hence the transient electric field shown in Fig. 13 in this spatial scale can be regarded as unchanged. Especially, the charge transport mechanism of positive charge is mainly discussed. As for negative charge, it is similar as positive charge, which can be analyzed as same expression by replacing E with $-E$.

According to charge transport dynamics, the one-dimensional expression of current density J_p is

$$J_p = \mu_p p E(t) - D_p \nabla p = \mu_p p E(t) - D_p \frac{\partial p}{\partial x} \tag{2}$$

where, p is the concentration of positive charge, μ_p and D_p are mobility and diffusion coefficient, respectively. Moreover, the positive direction of E is same as coordinate x.

Then, as described in Fig. 15(a), the conservation equation of positive charge can be

$$D_p \frac{\partial^2 p}{\partial x^2} - \mu_p E(t) \frac{\partial p}{\partial x} - \frac{p}{\tau} = \frac{\partial p}{\partial t} \tag{3}$$

where τ is the lifetime of positive charge. The change of positive charge can be attributed to thee sources: the first term is related the diffusion of positive charge; the second term is related to the

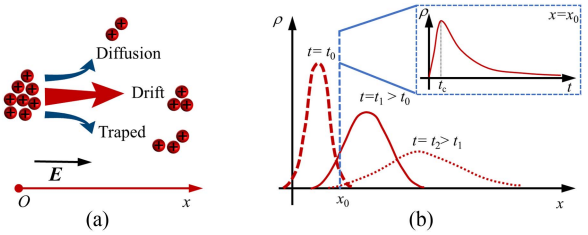

Fig. 15. Charge transport dynamics of generate of PD pulse current. (a) Charge transport schematic. (b) Transport process of charge.

drift of positive charge caused by the electric field; and the third term is related to the capture of traps.

When the electric field strength E exceeds the discharge inception field strength, some positive charge will be excited by the high electric field strength [13], [14], [15]. The position where positive charge generated initially is defined as origin, as shown in Fig. 15(a) and this moment is defined as 0 s. So, there is

$$p(x,0) = g \cdot \delta(x) \tag{4}$$

where, $p(x,0)$ is the distribution of positive charge at 0 s, g is the generation rate and δ is the Dirac function.

By replacing $p(x,0)$ as

$$p(x,t) = \exp(-t/\tau) \cdot \xi(x,t). \tag{5}$$

Equation (3) transformed as

$$D_p \frac{\partial^2 \xi}{\partial x^2} - \mu_p E(t) \frac{\partial \xi}{\partial x} = \frac{\partial \xi}{\partial t}. \tag{6}$$

Be Laplace's transform, the distribution of p is finally acquired as

$$p(x,t) = \frac{g}{2\sqrt{\pi D_p t}} \exp\left(-\frac{t}{\tau}\right) \exp\left[-\frac{(x-\mu_p E(t)t)^2}{4D_p t}\right]. \tag{7}$$

Based on the (7), the schematic of distribution of p over time is given as red lines in Fig. 15(b). Influenced by the electric field, positive charge transport according to the direction of electric field. Besides, caused by capture of traps and the effect of diffusion, the amplitude of distribution of p gradually decreases with time. If the observed point is set at $x = x_0$, the charge density changes over time is also given in the blue dashed box. It can be found that the charge density increases sharply and then decreases slowly over time, which is similar as the PD pulse. From (2), the current density can be acquired

$$J_p(x,t) = \frac{g\left(\mu_p E(t) + x/2t\right)}{4\sqrt{\pi D_p t}} \exp\left(-\frac{t}{\tau}\right) \times \exp\left[-\frac{(x-\mu_p E(t)t)^2}{4D_p t}\right] \tag{8}$$

which has the similar monotonicity as p.

According to Fig. 15 and (8), for positive charges, when the electric field E is along the positive x-axis, the drift direction of the charges is also along the positive x-axis, resulting in a positive current density J_p. Conversely, when E is along the negative x-axis, the charges drift in the negative direction, and the coordinate x also increases in the negative direction, leading to a negative current density J_p. Therefore, the direction of the current density is consistent with the direction of the electric field E. So, it can be found that the polarity of PD pulse current depends on the direction of electric field.

TABLE IV
PARAMETERS FOR POSITIVE CHARGE IN SILICONE GEL [23]

Parameters	Values
μ_p(m^2/V·s)	3×10^{-8}
D_p(m^2/s)	3×10^{-9}
x=x_0(μm)	0.06
τ(s)	3×10^{-7}

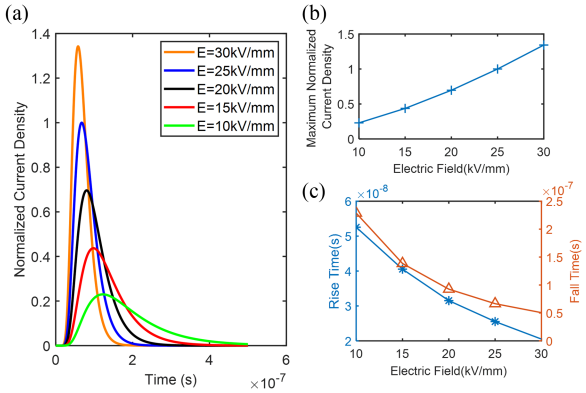

Fig. 16. PD pulse current density under different electric field strength. (a) Waveform of PD. (b) Amplitude of PD current density. (c) Rise and fall time.

Because PD usually occurs at the silicone gel side, the corresponding parameters in silicone gel given in Table IV are taken for the calculation of (8). Moreover, under the range of electric field strength from 10 to 30 kV/mm, the influence of electric field on PD pulse parameters is given in Fig. 16. Moreover, the generation rate g is unchanged in calculation and the current density is normalized by the maximum amplitude of current density under 25 kV/mm.

From Fig. 16(b), it can be found that the amplitude of current density linearly increases with the increase in electric field strength. In general, the generation rate g will increase in a power-law manner with increase in electric field, and hence amplitude of current density actually increases in a power-law manner with electric field strength. Moreover, the quantity of trapped charge during the whole process of PD can be simply seen to increase in a power-law manner with electric field strength.

Furthermore, the rise and fall times of current density are also extracted. As shown in Fig. 16(c), the rise time decreases with the increase in electric field strength while fall time exhibits an exponential decay with increase in electric field strength under the range of 10 to 30 kV/mm.

Therefore, from (8), the influence of electric field on PD pulse parameters can be acquired. It should be noted that the trapped charge in the transport process will also influence electric field. As shown in Fig. 15(a), the electric field caused by trapped

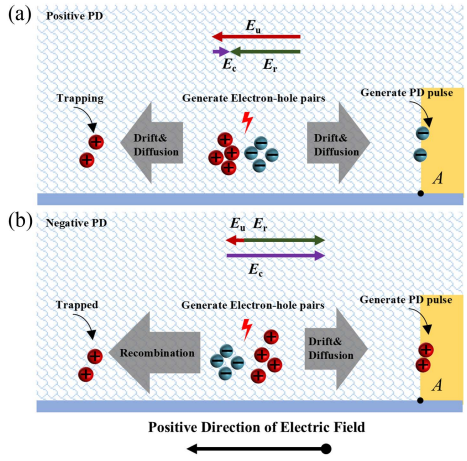

Fig. 17. Theory analysis of mechanism of PD at point A of DBC over time. (a) Positive PD. (b) Negative PD.

positive charge is opposite to the original electric field and it decreases the drift electric field strength. Thus, the electric field caused by trapped charge should also be taken into consideration which is discussed in the following subsection.

Overall, this analytical solution is applicable to the PD transport process at the nanometer–micrometer scale, under the assumption of a spatially uniform electric field. It focuses on one-dimensional positive charge transport in silicone gel, incorporating drift, diffusion, and trapping effects.

C. Theory Analysis of Evolution Mechanism of PD of DBC

As mentioned above, the component E_c attributed to the trapped charge caused by the transport process of PD can also modulate the electric field. The total electric field could be the sum of these two components

$$E_r = E_c + E_u. \tag{9}$$

As for E_u, it is the electric field caused by the externally applied voltage and the relaxation process induced by the material properties and structure, which can be calculated accurately as discussed in Section IV-A. As for E_c, it is difficult to be calculated, because E_c not only depends on the previous discharge but also the microscopic process in materials. For the sake of analysis, E_c is used for qualitative analysis of mechanism explanation.

Moreover, as the experimental results given in Fig. 11, the apparent charge amount of positive and negative PD pulses is basically the same. This means that the charge injected into the silicone gel during the rise edge stage will essentially be withdrawn during the fall edge stage, in each cycle of rectangle-wave. So, at rise edge stage, the effect of E_c can be ignored and hence the electric field is dominated by the E_u which is along the positive direction of electric field. Furthermore, according to simulation results, due to the high electric field strength near point A, the E_r at rise edge stage near point A is larger than other places and many more positive PDs are located near point A. So, taking point A for analysis, the schematic of electric field of positive PDs at the rise edge stage is given in Fig. 17(a).

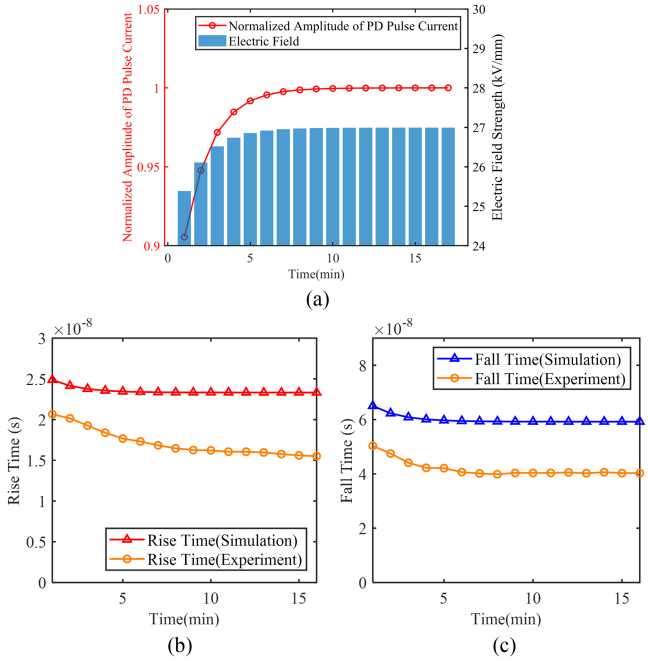

Fig. 18. Calculation results of parameters of PDs over time based on (8). (a) Normalized amplitude of PD pulse current density. (b) Rise time. (c) Fall time.

As for fall edge stage, because of the decrease of E_u, E_r is dominated by the E_c, which is along the negative direction of electric field. Because of many positive PDs located near point A in the rise edge stage, there will be much more trapped charge density is generated near point A and hence E_c at point A remains significantly higher than other locations. Similarly, at the fall edge stage, the schematic of electric field of negative PDs at point A is given in Fig. 17(b).

According to above analysis, the positive PDs are driven by E_u which is along the positive direction, while negative PDs depend on E_c which is along the negative direction. Because of different driven electric field of these two types PDs, the semi-quantitative mechanistic explanation of the evolution characteristics of positive and negative polarity PDs during the transitional period is separately discussed below.

1) Positive PD at Rise Edge Stage: As for the initial characteristics, at the rise edge stage, with the increase in voltage, when E_r exceeds the inception electric field, the positive and negative charge pairs are generated and then separated by the positive electric field, as shown in Fig. 17(a). During this process, the corresponding positive charges drift under the electric field and then are trapped. The negative charges are transported to electrode to generate the positive PD pulse current.

As for the evolution characteristics during the transitional period, by taking the evolution characteristic of the electric field strength shown in Fig. 14(a) into (8), the relaxation process of electric field is taken into consideration. In this case, the evolution characteristics of detailed waveform parameters (normalized PD pulse current amplitude, rise time, and fall time) of positive PDs are calculated and then shown in Fig. 18. Moreover, for the sake of comparation, the experimental results in Fig. 10 are also painted in Fig. 18.

It can be found that influenced by the relaxation process of electric field, the amplitude of positive PDs also increases over time and becomes steady after 9 min as shown in Fig. 18(a), which corresponds well with the experimental results shown in Figs. 7(b) and 9(a).

Moreover, as shown in Fig. 18(b) and (c), the rise time (t_r) and fall time (t_f) of the PD pulse current decrease over time and then become unchanged after 9 min, due to the change of electric field strength. These trends correspond well with the experimental results which get from Fig. 10. Moreover, the magnitudes of rise time and fall time acquired from simulation and (8) are the same as the range of their magnitudes in experimental results got from Fig. 10.

These results reflect the effectiveness of (8). More importantly, it can be found that the change of electric field strength caused by the relaxation effect is one of the key driving forces of the evolution of positive PD characteristics.

2) Negative PD at Fall Edge Stage: As for the initial characteristics, at the fall edge stage, with the decrease of voltage, the E_r is gradually dominated by E_c, when E_r exceeds the inception electric field, the positive and negative charge pairs are generated and then separated by the negative electric field, as shown in Fig. 17(b). During this process, the corresponding positive charges are transported to electrode under the negative electric field and then generate the negative PD pulse current. The negative charges are transported to neutralize the trapped charges.

As for the evolution characteristics during the transitional period, because E_c mainly depends on the quantity of trapped charge while trapped charge are generated in positive PD process, according to analysis of positive PDs, the quantity of trapped charge also increases over time and then becomes steady after 9 min. Thus, at the fall edge stage, the change of electric field E_c over time shows the same behavior. It is noted that when at fall edge stage, the large quantity of trapped charge will lead to a strong localized electric field strength and hence the change of externally applied electric field can be ignored, as shown in Fig. 17(b). So, electric field E_r also increases over time and then becomes steady after 9 min at the fall edge stage.

On the basis, according to (8), influenced by the change of electric field strength, the amplitude of negative polarity PD pulse will increase over time and then become unchanged after 9 min. This can explain the experimental results shown in Figs. 7(c) and 9(b). As for the detailed characteristics, with the increase in electric field strength, according (8) and Fig. 16(c), the rise time will decrease, which corresponds to experimental results shown in Fig. 10(a). As for fall time, because of localized higher electric field strength E_c, according to Fig. 16(c), the variation in fall time is minimal under localized high electric field strength, which accounts for experimental results shown in Fig. 10(b).

Consequently, it can be found that the change of transient electric field caused by the Maxwell-Wagner relaxation effect at the rise edge stage is the main possible reason for the change in PD evolution characteristics.

Furthermore, if the increase in electric field strength caused by the relaxation effect at the rise edge stage is suppressed, the corresponding increase in PD amplitude can also be suppressed. For example, by adjusting the conductivity of the insulating material, the transient evolution of the peak electric field changes from increasing to decreasing with time. Besides, reducing the effective lifetime of charges near the triple junction, the local PD pulse current amplitude can also be suppressed, as described by (8). These methods will provide more better insulation design in the future.

V. Conclusion

In this article, the detailed PD evolution characteristics of DBC and underlying discharge mechanisms during the transitional period under positive polarity rectangle-wave voltage are presented and analyzed. More importantly, a systematic analysis theory for the PD detailed characteristics under the influence of electric field relaxation is proposed. There are four conclusions in this article.

1) The detailed PD evolution characteristics of DBC over time are acquired by shunt-resistor-based current measurement method. The amplitude of positive and negative PDs over time both increase gradually at first and then reach a stable state until 9 min. Moreover, the rise time for both positive and negative PD pulses exhibit exponential decay over time and the change gradually levels off after 9 min. The fall time of positive pulses exhibit exponential decay over time and the change gradually levels off after 9 min, but the fall time for negative pulses basically unchanged over time.
2) Then, through transient electric field simulation, the relaxation process of the electric field is revealed. At the end of the rise edge stage of each cycle, the electric field strength at point A (maximum electric field position) increases as the number of cycles increases. After approximately 9 min, the electric field strength at point A remains essentially unchanged.
3) Furthermore, within the frame of charge transport dynamics, analytical formula of PD pulse current is proposed in which the PD waveform parameters are connected with the electric field and other detail parameters of materials. It can be found that the rise and fall time decrease and amplitude of PD pulse increases with the increase of electric field.
4) Based on the transient electric field simulation considering the relaxation effect, along with the analytical formula of the PD pulse current, a reasonable evolution mechanism for PD during the transitional period is proposed. The mechanism explanation can account for most of the experimental results. Most importantly, it points out that the key factor governing this transitional process is the relaxation of the electric field during the rise edge stage.

References

[1] T. Van Do, J. P. F. Trovão, K. Li, and L. Boulon, "Wide-bandgap power semiconductors for electric vehicle systems: Challenges *and* trends," *IEEE Veh. Technol. Mag.*, vol. 16, no. 4, pp. 89–98, Dec. 2021.

[2] R. Ravindran and A. M. Massoud, "An overview of wide and ultra wide bandgap semiconductors for next-generation power electronics applications," *Microelectron. Eng.*, vol. 299, no. 5, pp. 1–22, Sep. 2025.
[3] Y. Ding, Y. Wang, H. Sun, and Y. Yin, "High-temperature partial discharge characteristics of power module packaging insulation under rectangle pulse with high dV/dt based on down-mixing method," *IEEE Trans. Ind. Electron.*, vol. 70, no. 7, pp. 7334–7342, Jul. 2023.
[4] J. Drechsel, H. Barth, and L. Rebenklau, "Partial discharge analyses of DBC substrates," in *Proc. PCIM Eur.*, May 2023, pp. 1–6.
[5] Z. Zhang, K. D. T. Ngo, and G.-Q. Lu, "Characterization of a nonlinear resistive polymer-nanoparticle composite coating for electric field reduction in a medium-voltage power module," *IEEE Trans. Power Electron.*, vol. 37, no. 3, pp. 2475–2479, Mar. 2022.
[6] Y. Gao et al., "Impacts of the bottom copper layer of direct-bond copper substrates on the partial discharge performance in power modules," *IEEE Trans. Power Electron.*, vol. 40, no. 4, pp. 5999–6009, Apr. 2025.
[7] M. Ghassemi, "PD measurements, failure analysis, and control in high-power IGBT modules," *High Voltage*, vol. 3, no. 3, pp. 170–178, Sep. 2018.
[8] B. Zhang, Z. Yang, K. Li, X. Jiang, M. Yao, and X. Li, "Electrical tree failure at DBC substrate-silicone gel interface in high-voltage power module under positive rectangle-wave voltage," *IEEE J. Emerg. Sel. Topics Power Electron.*, vol. 12, no. 5, pp. 4967–4978, Oct. 2024.
[9] I. Semenov, T. Grav Aakre, I. Gunheim Folkestad, I. Smisethjell, K. Niayesh, and L. E. Lundgaard, "Partial discharge inception in ceramic substrates embedded in silicone liquid, silicone gel, and mineral oil at fast voltage rise and sinusoidal voltage," *IEEE Trans. Dielect. Elect. Insul.*, vol. 31, no. 4, pp. 1721–1728, Aug. 2024.
[10] I. Semenov, I. F. Gunheim, K. Niayesh, H. K. H. Meyer, and L. Lundgaard, "Investigation of partial discharges in AlN substrates under fast transient voltages," *IEEE Trans. Dielectr. Elect. Insul.*, vol. 29, no. 2, pp. 745–752, Apr. 2022.
[11] H. You, Z. Wei, B. Hu, Z. Zhao, R. Na, and J. Wang, "Partial discharge behaviors in power modules under rectangle pulses with ultrafast dv/dt," *IEEE Trans. Power Electron.*, vol. 36, no. 3, pp. 2611–2620, Mar. 2021.
[12] L. Wang, Z. Zeng, P. Sun, S. Ai, J. Zhang, and Y. Wang, "Electric-field-dominated partial discharge in medium voltage SiC power module packaging: Model, mechanism, reshaping, and assessment," *IEEE Trans. Power Electron.*, vol. 37, no. 5, pp. 5422–5432, May 2022.
[13] X. Liu et al., "Characteristics and identification of partial discharge for insulation structures in high voltage IGBT modules under positive rectangle-wave voltage," *IEEE Trans. Power Electron.*, vol. 38, no. 4, pp. 5347–5359, Apr. 2023.
[14] C. Li et al., "Surface discharge characteristics of silicone gel and DBC under positive repetitive rectangle voltage," *Power Electron. Devices Compon.*, vol. 3, no. 3, pp. 1–10, Oct. 2022.
[15] H. You et al., "Partial discharge behaviors in power module under very high dV/dt repetitive rectangle voltages," in *Proc. IEEE Elect. Insul. Conf.*, Jun. 2019, pp. 489–492.
[16] Y. Ding, Y. Wang, M. Chen, L. Fan, and Y. Yin, "Aging and lifetime of power module packaging insulation due to partial discharge under high dV/dt rectangle-wave voltage and high temperature," *IEEE Trans. Power Electron.*, vol. 40, no. 7, pp. 9864–9875, Jul. 2025.
[17] L. Wang et al., "A review of partial discharge in medium voltage SiC power modules under rectangle-wave excitation: Characterization, mitigation, and detection," *IEEE J. Emerg. Sel. Topics Power Electron.*, vol. 12, no. 4, pp. 3588–3606, Aug. 2024.
[18] M. Chen, Y. Wang, L. Fan, Y. Ding, and Y. Yin, "Temperature-dependent local electric field transient analysis and measurement in high-voltage power module packaging," *IEEE Trans. Dielect. Elect. Insul.*, vol. 32, no. 4, pp. 2229–2238, Aug. 2025.
[19] M. Chen, Y. Wang, and Y. Yin, "Transient electric field dynamics of high-voltage power module packaging insulation at high temperatures," in *Proc. IEEE 6th Int. Electr. Energy Conf.*, May 2023, pp. 3241–3246.
[20] T. Wen et al., "Time-domain finite element method for transient electric field and transient charge density on dielectric interface," *CSEE J. Power Energy Syst.*, vol. 8, no. 1, pp. 143–154, Jan. 2022.
[21] J. Mohammed et al., "Enhanced dielectric and optical properties of nanoscale barium hexaferrites for optoelectronics and high frequency application," *Chin. Phys. B*, vol. 27, no. 12, Dec. 2018, Art. no. 128104.
[22] J. Xu, X. Li, X. Cui, Z. Zhao, S. Mo, and B. Ji, "Trap characteristics and their temperature-dependence of silicone gel for encapsulation in IGBT power modules," *CSEE J. Power Energy Syst.*, vol. 7, no. 3, pp. 614–621, May 2021.
[23] J. Xu, "Research and application on the electrical characteristics of silicone gel for the encapsulant of high-voltage high-power IGBT modules," Ph.D. dissertation, North China Elect. Power Univ., Beijing, China, 2021.
[24] *High-Voltage Test Techniques–Partial Discharge Measurements*, IEC Standard 60270-2015, 2015.
[25] X. Li et al., "Influence of bubbles on the discharge characteristics of silicone gel for high voltage module encapsulation under positive rectangle-wave voltage," (in Chinese), *Trans. China Electrot. Soc.*, vol. 38, no. 15, pp. 1–11, 2023.

Zhaocheng Liu was born in Hebei Province, China, in 1997. He received the B.Sc. degree in electrical engineering in 2019 from North China Electric Power University, Baoding, China, where he is currently working toward the Ph.D. degree in electrical engineering.

His main research interests include computational electromagnetics, electrical insulation, and packaging problems for high voltage power semiconductor device.

Xiang Cui (Senior Member, IEEE) was born in Baoding, Hebei Province, China, in 1960. He received the B.Sc. and M.Sc. degrees in electrical engineering from North China Electric Power University, Baoding, China, in 1982 and in 1984, respectively, and the Ph.D. degree in accelerator physics from the China Institute of Atomic Energy, Beijing, China, in 1988.

He is currently a Professor and the Vice Director of the State Key Laboratory of Alternate Electrical Power System with Renewable Energy Sources, North China Electric Power University. His research interests include computational electromagnetics, electromagnetic environment and electromagnetic compatibility in power systems, insulation and magnetic problems in high-voltage apparatus.

Dr. Cui is a Fellow of the Chinese Society for Electrical Engineering and a Fellow of the China Electrotechnical Society.

Xuebao Li was born in Tianjin, China, in 1988. He received the B.Sc. and Ph.D. degrees in electrical engineering from North China Electric Power University, Beijing, China, in 2011 and in 2016, respectively.

He is currently an Associate Professor with the School of Electrical and Electronic Engineering, North China Electric Power University. His research interests include the electromagnetic environment and electromagnetic compatibility in power systems, and insulation problems in high-voltage apparatus.

Weitong Xu was born in Anhui, China in 2003. He received the B.E.(B.Sc.) degree in electrical engineering from China Three Gorges University, Yichang, China, in 2024. He is currently working toward the Ph.D. degree in electrical engineering with the North China Electric Power University, Beijing, China.

His research interests include partial discharge in high voltage devices under the square wave.

Zhibin Zhao was born in Hebei, China, in 1977. He received the Ph.D. degree in electrical engineering from North China Electric Power University, Baoding, China, in 2005.

He is currently a Professor with the State Key Laboratory of Alternate Electrical Power System, Renewable Energy Sources, North China Electric Power University. His main research interests include computational electromagnetics and electromagnetic compatibility in power electronic.

Lei Qi was born in Nanyang, Henan, China, in 1978. He received the B.S., M.S., and Ph.D. degrees in electrical engineering from North China Electric Power University, Baoding, China, in 2000, 2003, and 2006, respectively.

He is currently a Professor of electrical engineering with North China Electric Power University. His research interests include electromagnetic fields theory and application, electromagnetic compatibility in power systems, and advanced power transmission technology.